JACS
JOURNAL OF THE AMERICAN CHEMICAL SOCIETY
Article
Cite This: J. Am. Chem. Soc. 2017, 139, 15363-15370
pubs.acs.org/JACS

M_2(*m*-dobdc) (M = Mn, Fe, Co, Ni) Metal–Organic Frameworks as Highly Selective, High-Capacity Adsorbents for Olefin/Paraffin Separations

Jonathan E. Bachman,[†,∥] Matthew T. Kapelewski,[‡,∥] Douglas A. Reed,[‡] Miguel I. Gonzalez,[‡] and Jeffrey R. Long*[,†,‡,§]

[†]Department of Chemical & Biomolecular Engineering, and [‡]Department of Chemistry, University of California, Berkeley, California 94720, United States

[§]Materials Sciences Division, Lawrence Berkeley National Laboratory, Berkeley, California 94720, United States

Supporting Information

ABSTRACT: The metal–organic frameworks M_2(*m*-dobdc) (M = Mn, Fe, Co, Ni; *m*-dobdc^{4-} = 4,6-dioxido-1,3-benzenedicarboxylate) were evaluated as adsorbents for separating olefins from paraffins. Using single-component and multicomponent equilibrium gas adsorption measurements, we show that the coordinatively unsaturated M^{2+} sites in these materials lead to superior performance for the physisorptive separation of ethylene from ethane and propylene from propane relative to any known adsorbent, including *para*-functionalized structural isomers of the type M_2(*p*-dobdc) (*p*-dobdc^{4-} = 2,5-dioxido-1,4-benzenedicarboxylate). Notably, the M_2(*m*-dobdc) frameworks all exhibit an increased affinity for olefins over paraffins relative to their corresponding structural isomers, with the Fe, Co, and Ni variants showing more than double the selectivity. Among these frameworks, Fe_2(*m*-dobdc) displays the highest ethylene/ethane (>25) and propylene/propane (>55) selectivity under relevant conditions, together with olefin capacities exceeding 7 mmol/g. Differential enthalpy calculations in conjunction with structural characterization of ethylene binding in Co_2(*m*-dobdc) and Co_2(*p*-dobdc) *via in situ* single-crystal X-ray diffraction reveal that the vast improvement in selectivity arises from enhanced metal–olefin interactions induced by increased charge density at the metal site. Moderate olefin binding enthalpies, below 55 and 70 kJ/mol for ethylene and propylene, respectively, indicate that these adsorbents maintain sufficient reversibility under mild regeneration conditions. Additionally, transient adsorption experiments show fast kinetics, with more than 90% of ethylene adsorption occurring within 30 s after dosing. Breakthrough measurements further indicate that Co_2(*m*-dobdc) can produce high purity olefins without a temperature swing, an important test of process applicability. The excellent olefin/paraffin selectivity, high olefin capacity, rapid adsorption kinetics, and low raw materials cost make the M_2(*m*-dobdc) frameworks the materials of choice for adsorptive olefin/paraffin separations.

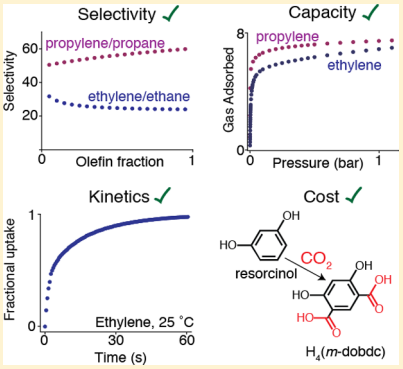

INTRODUCTION

Olefins, including ethylene and propylene, are high-value products obtained primarily from naphtha or ethane cracking and are ubiquitous feedstocks for the most commonly used polymers.[1] However, olefins are produced as a mixture with their saturated paraffinic counterparts. Separations of these olefin/paraffin mixtures are some of the most energy-intensive industrial processes and are currently dominated by cryogenic distillation technologies.[1,2] The U.S. alone consumes over 120 TBtu/yr in carrying out olefin/paraffin separations.[3,4] Non-thermally driven processes, such as adsorption, can dramatically reduce the cost and energy required to purify olefins.[5] However, replacing distillation requires adsorbents with adequate performance characteristics, including selectivity, capacity, kinetics, and cost. While there have been significant research efforts directed toward designing materials with the requisite olefin/paraffin separation properties, usually operating via size-selective,[6−10] chemisorptive,[11−17] or physisorptive[18−22] mechanisms, better performing materials are still needed.

Metal–organic frameworks are a class of porous crystalline materials with a high degree of structural tunability that have been demonstrated to be capable of facilitating gas separations through each of these three mechanisms.[23−26] Due to the small and similar kinetic diameters of light olefins and paraffins, size-selective adsorbents typically display moderate selectivities alongside a very low working capacity and slow kinetics. These characteristics arise from the narrow pore sizes necessary to discriminate between small molecules. For example, NbOF-FIVE-Ni, a metal–organic framework in which Ni^{2+}-pyrazine square grids are pillared by $[NbOF_5]^{2-}$ units to form 4.752(1) Å channels that accommodate propylene but reject propane, displays near perfect propylene/propane selectivity but is

Received: June 20, 2017
Published: October 5, 2017

DOI: 10.1021/jacs.7b06397
J. Am. Chem. Soc. 2017, 139, 15363−15370

impaired by a very low (0.6 mmol/g) working capacity.[10] Chemisorptive mechanisms, such as π-complexation with Ag(I) or Cu(I), appear promising due to the high binding enthalpy for olefins.[27] However, these high selectivities arise from metal−olefin interactions that are typically greater than 100 kJ/mol in strength, leading to irreversible binding under typical temperature swing or pressure swing adsorption conditions. By exchanging Ag(I) into the porous aromatic framework PAF-1-SO_3H,[28] Li and co-workers showed high ethylene/ethane selectivity using the 106 kJ/mol binding affinity between the olefin and Ag(I); however, they could not demonstrate reversibility under process conditions.[12] Finally, adsorbents that display separation properties based on physisorptive mechanisms typically have faster cycling kinetics and better working capacities due to larger pore sizes and weaker binding affinities. However, due to the difficulty in discriminating between olefins and paraffins, adsorbents have not yet displayed sufficient selectivity to produce polymer grade (99.9% purity) olefins.[29]

The metal−organic frameworks M_2(*p*-dobdc) (M-MOF-74; CPO-27-M; M = Mg, Mn, Fe, Co, Ni, Zn; *p*-dobdc^{4-} = 2,5-dioxido-1,4-benzenedicarboxylate),[30−32] which feature ∼12 Å-wide hexagonal channels lined with a high concentration of exposed divalent cations, use coordinatively unsaturated M^{2+} sites to polarize and adsorb olefins preferentially over paraffins.[18,19,33] Among these materials, Fe_2(*p*-dobdc) shows an ethylene/ethane selectivity of ∼14 at 45 °C with an ethylene capacity of greater than 7 mmol/g, and Mn_2(*p*-dobdc) shows a propylene/propane selectivity of ∼16 with a propylene capacity of greater than 7.5 mmol/g. While these frameworks show reversible olefin adsorption with olefin capacities that are more than an order of magnitude higher than in size-selective adsorbents, improvements in selectivity are desired in order to boost olefin purity in the product stream. Such increases in selectivity would translate to olefin purities sufficient for downstream processes, such as polymerization.

We hypothesized that higher selectivities could be achieved in these physisorptive materials by altering the affinity of the metal site for adsorbed hydrocarbons. By employing a *meta*-substituted H_4(*m*-dobdc) ligand, a structural isomer M_2(*m*-dobdc) (M = Mg, Mn, Fe, Co, Ni; *m*-dobdc^{4-} = 4,6-dioxido-1,3-benzenedicarboxylate) can be formed. This metal−organic framework has been shown to have increased charge density at the metal sites, leading to enhanced H_2 binding enthalpies and greater H_2 storage capacities.[34] Further, this metal−organic framework is produced from low-cost raw materials, as its linker is derived from a reaction of CO_2 with the commodity chemical resorcinol, lending itself to large-scale industrial applications.[35] The present study aims to evaluate a series of M_2(*m*-dobdc) metal−organic frameworks for utility in olefin/paraffin separations using single-component equilibrium gas adsorption, multicomponent equilibrium gas adsorption, adsorption kinetics, transient breakthrough measurements, and *in situ* single-crystal X-ray diffraction experiments. From this, we have found that the M_2(*m*-dobdc) frameworks exhibit superior performance to their *para*-functionalized counterparts (M_2(*p*-dobdc)) and the highest selectivity values among materials that utilize a fast, reversible, physisorptive mechanism. Most notably, Fe_2(*m*-dobdc) shows an ethylene/ethane selectivity of ∼25 and a propylene/propane selectivity of ∼55 under relevant conditions, demonstrating that control over the electronic properties of the open metal sites can lead to improved performance. This is a generalizable concept, in that tuning the electronic environment around a given adsorption site in a given structure can greatly affect adsorption and separation properties. The combined features of these adsorbents including selectivity, capacity, kinetics, and cost, make the M_2(*m*-dobdc) compounds promising adsorbents for industrial olefin/paraffin separations, and these materials have the potential to offset significant energy consumption relative to the decades-old distillation technology that is employed today.

MATERIALS AND METHODS

Synthesis of M_2(*m*-dobdc) (M = Mn, Fe, Co, Ni). The M_2(*m*-dobdc) materials were synthesized according to modified versions of the large-scale literature procedures.[33] $MnCl_2$, $FeCl_2$, $CoCl_2$, and $NiCl_2$ were purchased from Sigma-Aldrich and used as received. Methanol was purchased from EMD Millipore Corporation as DriSolv grade, dried over 3 Å sieves, and sparged with Ar prior to use. Dimethylformamide (DMF) was purchased from EMD Millipore Corporation as OmniSolv grade, sparged with Ar, and dried with an alumina column prior to use.

Co_2(*m*-dobdc) and Ni_2(*m*-dobdc). A mixture of 310 mL of methanol and 310 mL of DMF was added to a 1-L three-neck round-bottom flask equipped with a reflux condenser and purged with N_2 while stirring for 1 h. The ligand H_4(*m*-dobdc) (2.00 g, 10.1 mmol) and $CoCl_2$ (3.27 g, 25.2 mmol) or $NiCl_2$ (3.27 g, 25.2 mmol) were added to the solvent under N_2 pressure, and the reaction mixture was heated at 120 °C for 18 h while stirring vigorously. The mixture was cooled to ambient temperature and then filtered, yielding a microcrystalline powder. The resulting powder was rinsed with DMF, and soaked in 200 mL of DMF at 120 °C for 24 h. The powder was collected by filtration, rinsed with methanol, and soaked in 200 mL of methanol at 60 °C for 12 h. The supernatant solution was decanted, and 200 mL of fresh methanol were added. This procedure was repeated four times, such that the total time washing with methanol was 2 days. This resulted in an ∼54% yield of Co_2(*m*-dobdc) and Ni_2(*m*-dobdc). The resulting powder was collected by filtration and heated at 180 °C under dynamic vacuum (<0.01 mbar) for 24 h. The resulting activated powders were purple and brown for Co_2(*m*-dobdc) and Ni_2(*m*-dobdc), respectively.

Mn_2(*m*-dobdc) and Fe_2(*m*-dobdc). All manipulations involving the preparation and handling of Mn_2(*m*-dobdc) and Fe_2(*m*-dobdc) were performed under a N_2 atmosphere in a VAC Atmospheres glovebox or using standard Schlenk techniques. A solution of MCl_2 (2.5 equiv, 3.0 mmol) in 12 mL of methanol was added to a 200 mL Schlenk flask charged with a magnetic stir bar and a solution of H_4(*m*-dobdc) (240 mg, 1.0 equiv, 1.2 mmol) in 68 mL of DMF. The solution was stirred at 120 °C for 18 h. The resulting powder was collected by filtration, rinsed with DMF, and soaked in 20 mL of DMF at 120 °C for 24 h. The powder was collected by filtration, rinsed with methanol, and soaked in 20 mL of methanol at 60 °C for 12 h. The supernatant solution was decanted, and 10 mL of fresh methanol were added. This process was repeated four times, such that the total time washing with methanol was 2 days. This resulted in an ∼75% yield for Mn_2(*m*-dobdc) and an ∼85% yield for Fe_2(*m*-dobdc). The resulting powder was collected by filtration and heated at 180 °C under dynamic vacuum (<0.01 mbar) for 24 h. The resulting activated powders were light purple and light pink for Fe_2(*m*-dobdc) and Mn_2(*m*-dobdc), respectively.

Single-Component Gas Adsorption Measurements. Single-component gas adsorption experiments in the pressure range of 0−1.1 bar were conducted on a Micromeritics 3Flex instrument, which uses a volumetric method to determine the amount adsorbed under an equilibrated gas pressure. Activated samples were transferred under a dry N_2 atmosphere into preweighed sample tubes and then capped with a Micromeritics TranSeal. Samples were then evacuated at 180 °C under a dynamic vacuum of $<10^{-5}$ bar, until the off-gas rate was less than 10^{-7} bar/s. The mass of the activated sample was then recorded, typically in the range 50−150 mg. Prior to collecting each adsorption isotherm, the free-space of the sample was measured using UHP (99.999%) He. Gas adsorption isotherms of ethylene, ethane,

DOI: 10.1021/jacs.7b06397
J. Am. Chem. Soc. 2017, 139, 15363−15370

propylene, and propane were measured at 25, 35, and 45 °C using a water bath to maintain a constant temperature. Samples were reactivated in between each isotherm measurement by heating at 180 °C under dynamic vacuum for 2 h. Oil-free vacuum pumps and oil-free pressure regulators were used for all measurements.

Isotherm Fitting, Ideal Adsorbed Solution Theory, and Differential Enthalpies. The single-component gas adsorption isotherms were fit using a dual-site Langmuir−Freundlich equation, given by

$$n = \frac{q_{\mathrm{sat,a}} b_{\mathrm{a}} P^{\nu_{\mathrm{a}}}}{1 + b_{\mathrm{a}} P^{\nu_{\mathrm{a}}}} + \frac{q_{\mathrm{sat,b}} b_{\mathrm{b}} P^{\nu_{\mathrm{b}}}}{1 + b_{\mathrm{b}} P^{\nu_{\mathrm{b}}}} \quad (1)$$

where n is the amount adsorbed in mmol/g, q_{sat} is the amount adsorbed when saturated with the gas in mmol/g, b is the Langmuir parameter in bar^{-1}, P is the gas pressure in bar, ν is the dimensionless Freundlich parameter, and subscripts a and b correspond to two different site identities. These parameters were determined using a least-squares method and are given in Supplementary Tables 1−4. Ideal Adsorbed Solution Theory (IAST) was used to determine adsorbent selectivities from single-component gas adsorption isotherms.[36−38] This involves numerically solving for the spreading pressure and subsequently determining the composition of the adsorbed phase at a given gas phase composition. The selectivity is then given by

$$S = \frac{x_{\mathrm{olefin}}/x_{\mathrm{paraffin}}}{y_{\mathrm{olefin}}/y_{\mathrm{paraffin}}} \quad (2)$$

where S is the IAST selectivity, x is the mole fraction in the adsorbed phase, and y is the mole fraction in the gas phase. Finally, the differential enthalpy was extracted from the temperature dependence of the isotherms using the Clausius−Clapeyron relationship.[39] The adsorption isotherm fits were numerically inverted and solved as $P(n)$. The differential enthalpy, h, can then be determined at a constant loading by

$$h = -R\frac{\mathrm{d}(\ln P)}{\mathrm{d}(1/T)} \quad (3)$$

where R is the ideal gas constant, P is the pressure at a given loading, and T is the temperature (298.15, 308.15, or 318.15 K) at which the isotherm data were collected.

Breakthrough Measurements. Breakthrough experiments were performed using a custom-built breakthrough apparatus, composed of primarily 1/8″ copper tubing fitted with Swagelok fittings and valves to control the flow of the gas to either flow through the sample holder or bypass the sample holder and flow directly to a gas chromatograph used to monitor outflow composition. A premixed 1:1 ethane/ethylene or 1:1 propane/propylene cylinder was attached to the breakthrough manifold via an MRS mass flow controller to control gas flow from the cylinder. A helium (99.999%) cylinder used to dilute the hydrocarbon mixture was also attached to the manifold and controlled by an MRS mass flow controller. A coil of tubing was placed after the mass flow controllers to ensure mixing of the gases. The Co_2(*m*-dobdc) sample was pelletized and broken into pieces using a 20−40 mesh sieve. Then, 0.575 g of the sample was loaded into one vertical component (13.335 cm, inner diameter of 0.4572 cm) of a U-shaped sample holder comprised of 1/4″ tubing and fitted with Swagelok VCR fittings with fritted (0.5 μm) gaskets to prevent the sample from moving. The U-shaped tubing was immersed in a sand-filled heating mantle and connected to the breakthrough manifold. The Co_2(*m*-dobdc) sample was activated in the sample holder by heating it in the sand bath at 180 °C under flowing He. The sample was then cooled to 45 °C for the breakthrough experiments. A total flow rate of 30 mL/min was employed, with each hydrocarbon mixture set to 2 mL/min and the He set to 28 mL/min. The uncertainty in the flow rate of the olefin/paraffin mixture is about 0.5 mL/min. The mixture was tested without flowing to the packed Co_2(*m*-dobdc) bed to ensure proper composition and separation using the GC monitoring the outflow. The mixture was then flowed through the packed bed of Co_2(*m*-dobdc), and the outflow was recorded by GC every 2.0 min for the ethane/ethylene mixture and every 3.5 min for the propane/propylene mixture. The outflow composition was analyzed by gas chromatography using an SRI Instruments 8610 V GC equipped with a 6′ HayeSep D column, which was kept at 90 °C. After both components for an experiment had broken through the packed Co_2(*m*-dobdc) bed, the flow was switched to He to fully desorb both hydrocarbon components from the column. The data were recorded and analyzed using PeakSimple software.

Single-Crystal X-ray Diffraction Experiments. *In situ* X-ray diffraction measurements for both Co_2(*m*-dobdc) and Co_2(*p*-dobdc) were performed on single crystals in ethylene-dosed capillaries, which were prepared according to a previously reported procedure.[40] Briefly, a methanol-solvated crystal of either Co_2(*m*-dobdc) or Co_2(*p*-dobdc) was mounted onto a borosilicate glass fiber using a minimal amount of epoxy, ensuring accessibility of the crystal pores. The glass fiber was then inserted into a 1.0 mm borosilicate glass capillary, which was connected to a capillary-dosing assembly attached to a port on a Micromeritics 3Flex instrument. The sample was evacuated under reduced pressure at 180 °C for 24 h to remove all solvent from the crystal. The capillary was dosed with 300 mbar of ethylene and then flame-sealed with a methane/oxygen torch.

X-ray diffraction data for all samples were collected at Beamline 11.3.1 at the Advanced Light Source at Lawrence Berkeley National Laboratory using synchrotron radiation (λ = 0.8856 Å for Co_2(*m*-dobdc)·2.0C_2H_4 and λ = 0.6888 Å for Co_2(*p*-dobdc)·1.9C_2H_4) and a Bruker PHOTON100 CMOS detector mounted on a D8 diffractometer. The samples were cooled to 100 K using an Oxford Cryosystems cryostream for data collection. For Co_2(*p*-dobdc)·1.9C_2H_4, the crystal was found to be an obverse/reverse twin based on analysis of the diffraction patterns, and CELL_NOW[41] was used to determine the orientation matrices. Raw data for each structure (using both twin matrices for Co_2(*p*-dobdc)·1.9C_2H_4) were integrated and corrected for Lorentz and polarization effects using the Bruker AXS SAINT[42] software and corrected for absorption using SADABS for Co_2(*m*-dobdc)·2.0C_2H_4 and TWINABS for Co_2(*p*-dobdc)·1.9C_2H_4.[43] For Co_2(*p*-dobdc)·1.9C_2H_4, TWINABS was used to produce a merged HKLF4 file for structure solution and initial refinement and an HKLF5 file for final structure refinement.

Structures were solved using either direct methods with SHELXS[44,45] (for Co_2(*p*-dobdc)·1.9C_2H_4) or intrinsic phasing methods for Co_2(*m*-dobdc)·2.0C_2H_4 with SHELXT[46] and refined using SHELXL[43,47] operated in the OLEX2 interface.[48] Thermal parameters were refined anisotropically for all non-hydrogen atoms. Disorder and thermal motion of the bound gas molecules required the use of displacement parameter and distance restraints. All framework H atoms were refined using the riding model. Hydrogen atoms on the coordinated ethylene molecules in Co_2(*m*-dobdc)·2.0C_2H_4 could not be located in the electron density difference map and were omitted from the refinement, but not the formula. Hydrogen atoms on the coordinated ethylene molecules in Co_2(*p*-dobdc)·1.9C_2H_4 were located in the electron density difference map, constrained to be coplanar with the ethylene carbon atoms, and restrained to have C−H distances based on those of free ethylene.

RESULTS AND DISCUSSION

Structural Characterization of Ethylene-Dosed Co_2(*m*-dobdc) and Co_2(*p*-dobdc). *In situ* single-crystal X-ray diffraction was employed as an initial means of comparing ethylene binding in the isomeric Co_2(*m*-dobdc) and Co_2(*p*-dobdc) frameworks. This technique requires large single crystals that can be manipulated and mounted, which restricts the method to the characterization of Co_2(*m*-dobdc) and Co_2(*p*-dobdc), the most crystalline of the M_2(dobdc) materials investigated here. However, relative differences between the two structures are expected to be similar in other variants. The structures of Co_2(*m*-dobdc) and Co_2(*p*-dobdc) under ∼0.3 bar of ethylene at 100 K (Figure 1) confirm that ethylene primarily

DOI: 10.1021/jacs.7b06397
J. Am. Chem. Soc. 2017, 139, 15363−15370

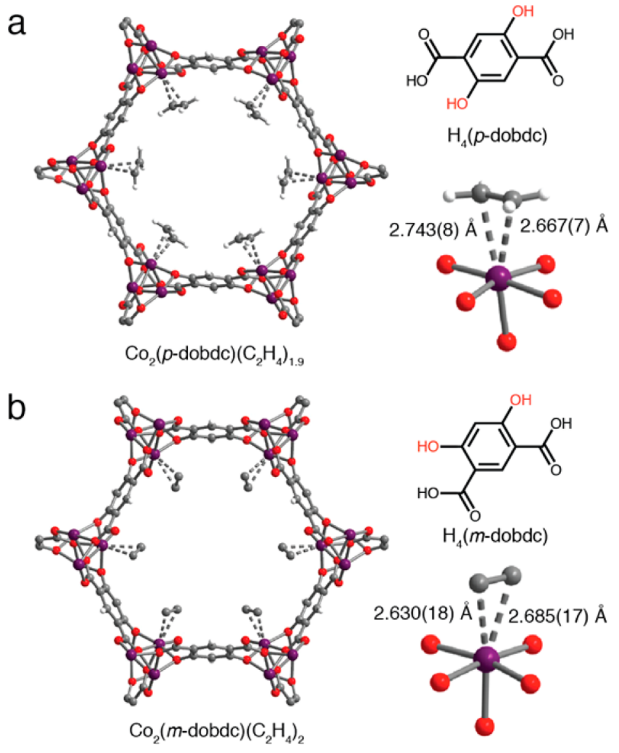

Figure 1. Comparison of the framework structures, ligand structure, and ethylene binding geometries for (a) Co_2(*p*-dobdc) and (b) Co_2(*m*-dobdc) under ~0.3 bar of ethylene at 100 K as determined from *in situ* single-crystal X-ray diffraction experiments. Purple, red, gray, and white spheres represent Co, O, C, and H atoms, respectively.

binds through a side-on interaction with the cobalt(II) sites in both materials. Unlike molecular Co−C_2H_4 complexes reported in the Cambridge Crystal Structure Database,[49] which feature low-spin cobalt(II) centers and Co−C distances in the range 1.965−2.087 Å, much longer Co···C distances are apparent in Co_2(*m*-dobdc)·2.0C_2H_4 (2.643(18) and 2.687(16) Å) and Co_2(*p*-dobdc)·1.9C_2H_4 (2.667(7) and 2.743(8) Å). These long distances indicate that the cobalt sites in both frameworks bind ethylene through much weaker reversible interactions compared to typical transition metal alkene complexes. Similar weak interactions have been reported for ethylene and propylene in Co_2(*p*-dobdc)[19] and Fe_2(*p*-dobdc)[18] and have been attributed to limited π backbonding from the high-spin metal(II) centers in these frameworks.

The shorter Co···C distances in Co_2(*m*-dobdc)·2.0C_2H_4 compared to Co_2(*p*-dobdc)·1.9C_2H_4 likely result from stronger ethylene binding induced by the increased charge density at the cobalt(II) site in Co_2(*m*-dobdc). A similar effect was also observed for H_2 binding to Co_2(*m*-dobdc), in structures obtained from *in situ* neutron powder neutron diffraction experiments, and this was attributed to a higher charge density at the metal site in the *meta*-substituted variant using density functional theory.[33] The stronger Co−C_2H_4 interactions inferred from shorter Co···C distances in Co_2(*m*-dobdc)·2.0C_2H_4 are more generally expected to correspond to an increased olefin/paraffin selectivity in the M_2(*m*-dobdc) frameworks compared to the M_2(*p*-dobdc) isomers, as discussed below.

Gas Adsorption and Olefin/Paraffin Selectivity in M_2(*m*-dobdc) Frameworks. In rigid frameworks with well-defined gas adsorption sites, single-component gas adsorption isotherms reveal a wide range of information about the thermodynamics of gas molecules interacting within the system. Single-component ethylene, ethane, propylene, and propane isotherms were therefore measured at 25, 35, and 45 °C in M_2(*m*-dobdc) (M = Mn, Fe, Co, Ni) (Figure 2a and 2b). These isotherms display steep adsorption behavior at low pressures, corresponding to strong interactions with the frameworks. Among the four gases, propylene adsorbs the strongest, followed by ethylene, then propane, and last ethane for each variant. This qualitative comparison suggests that all of these materials selectively adsorb olefins over paraffins. Further, the high densities of coordinatively unsaturated metal centers in these materials afford olefin saturation capacities in excess of 7 mmol/g. Note that the adsorption of one molecule per metal corresponds to a loading of 6.6, 6.5, 6.4, and 6.4 mmol/g for M = Mn, Fe, Co, and Ni, respectively.

Single-component isotherms can be used to understand the expected equilibrium properties of multicomponent systems by applying IAST to predict the composition of the adsorbed phase in the presence of a gas mixture.[35] The IAST model is expected to work accurately for this system, given the relatively rigid nature of the framework and the absence of significant interactions between adsorbates bound to the metal sites at low gas loadings. The IAST selectivities were obtained from single-component dual-site Langmuir−Freundlich fits (Figure 2c and 2d). As this method extrapolates the isotherm of the less strongly bound gas (in this case ethane and propane), obtaining realistic results depends on restricting the saturation capacity for these isotherms to reasonable values (Tables S1−S4). Otherwise, nonphysical trends in the IAST selectivities can arise and severe overestimations of the values can result.[9]

After taking these procedures into consideration, we observe an ethylene/ethane IAST selectivity in Fe_2(*m*-dobdc) of over 25 under equimolar feed conditions at a total pressure of 1 bar and 25 °C, making it the most selective physisorptive material for the separation. This selectivity corresponds to a composition in the adsorbed phase of 96% ethylene in equilibrium with an equimolar gas phase. Within only two equilibrium stages, in which the ethylene adsorbed from an equimolar mixture at equilibrium is then desorbed and subsequently equilibrated with the adsorbent a second time, an ethylene purity of greater than 99.9% can be achieved. This is the minimum purity required for a polymerization feed and can usually only be achieved through cryogenic methods.[29] Additionally, this separation is accomplished at near-ambient temperatures, with further improvements in selectivity expected at reduced temperatures. Propylene/propane selectivity in Fe_2(*m*-dobdc) is greater than 55 under the same conditions, corresponding to 98% of the adsorbed phase composed of propylene in the first equilibrium stage. Variants including Mn, Co, and Ni also display high adsorption selectivities of greater than 15 for ethylene/ethane and greater than 30 for propylene/propane.

To verify the applicability of IAST in predicting behavior under real mixtures, multicomponent equilibrium adsorption measurements were conducted (Figure S1). By dosing an ethylene/ethane mixture of known composition, determining the total amount of gas adsorbed at equilibrium, and measuring the equilibrium composition of the gas phase after adsorption using a mass spectrometer, the composition of the adsorbed phase can be determined. Indeed, samples of M_2(*m*-dobdc) (M = Fe, Co, Ni), when dosed with an equimolar mixture of ethylene and ethane, revealed significant enrichment of

DOI: 10.1021/jacs.7b06397
J. Am. Chem. Soc. 2017, 139, 15363−15370

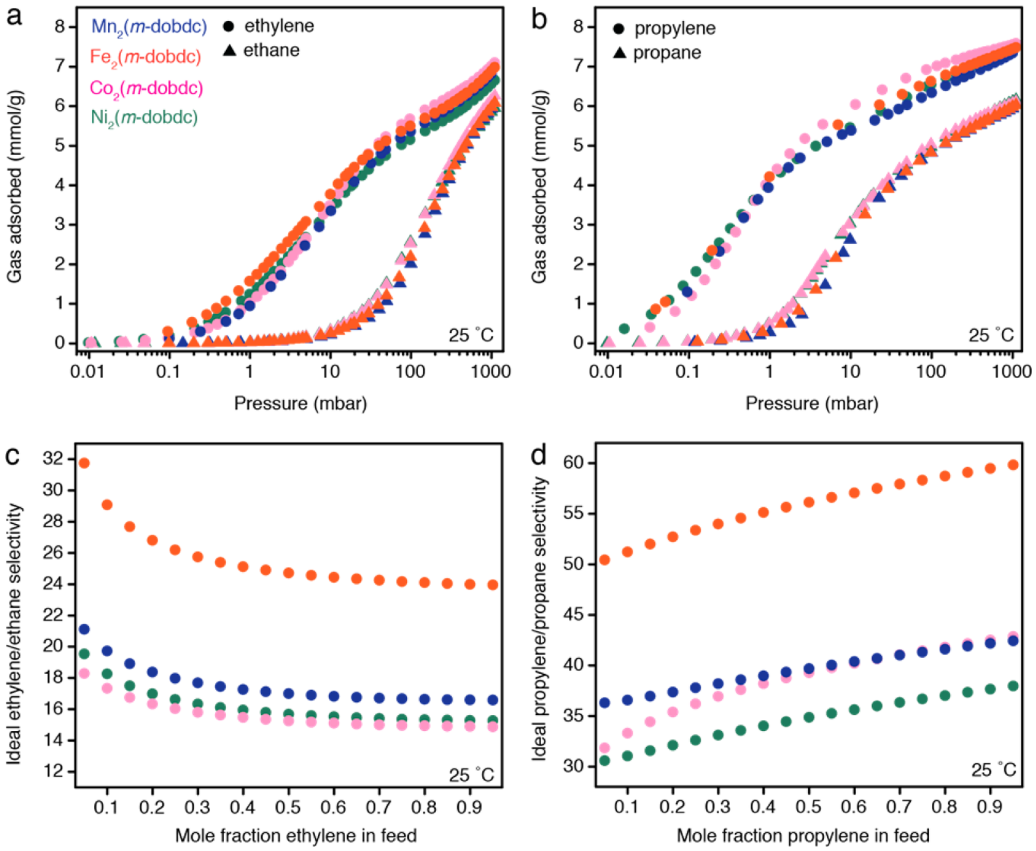

Figure 2. Single-component gas adsorption isotherms of (a) ethylene/ethane and (b) propylene/propane and their corresponding olefin/paraffin IAST selectivity for (c) ethylene/ethane and (d) propylene/propane at 25 °C in M_2(*m*-dobdc) (M = Mn, Fe, Co, Ni).

ethylene in the adsorbed phase. Additionally, equimolar ethylene/ethane breakthrough on Mn_2(*m*-dobdc) reveal its applicability under real gas conditions (Figure S11). Ethylene/ethane selectivities as determined from this method corroborate those calculated from IAST, with measured values of 25 ± 3 compared with 26, 14 ± 2 compared with 16, and 18 ± 2 compared with 16 for Fe_2(*m*-dobdc), Co_2(*m*-dobdc), and Ni_2(*m*-dobdc), respectively. This is not surprising, as the assumptions that are required for IAST to hold (the thermodynamic state of the adsorbent does not change upon gas adsorption, and adsorbate−adsorbate interactions are minimal, given they are isolated at discrete metal sites) are fulfilled in this system.

The IAST selectivities calculated at 45 °C for the M_2(*m*-dobdc) frameworks are significantly higher than those for the corresponding M_2(*p*-dobdc) isomers (Figure 3). In the case of ethylene/ethane, the most selective in the *para* series, Fe_2(*p*-dobdc), shows similar selectivity to Ni_2(*m*-dobdc), the least selective of the *meta* series. Additionally, Ni_2(*m*-dobdc) and Co_2(*m*-dobdc) have more than double the selectivity of their *para*-substituted counterparts. These changes are even more pronounced for a propylene/propane separation. All variants in the M_2(*m*-dobdc) series are significantly more selective than in the M_2(*p*-dobdc) series, and Fe_2(*m*-dobdc) has nearly triple the selectivity of Fe_2(*p*-dobdc). Moreover, temperature-dependent IAST calculations predict more dramatic differences in selectivity at lower temperatures, under which differences in adsorption enthalpy play a larger role in determining adsorption equilibria.

As the increased charge density at the metal site changes the relative adsorption enthalpies, it was not surprising to see improvements in olefin/paraffin adsorption selectivity; however, the magnitude of these changes was unexpected. Using the single-component isotherm fits and the Clausius−Clapeyron relationship, differential enthalpies of ethylene, ethane, propylene, and propane were determined as a function of loading (Figure 4). For ethylene and propylene, initial adsorption enthalpies below ∼1 mmol/g correspond to interactions between the gas and the metal site. The subsequent decrease in differential enthalpy for these species corresponds to saturation of the metal sites, and the enthalpies beyond this point result from subsequent binding sites. For ethane and propane, the initial adsorption at low loading also corresponds to interactions with the metal sites. However, increases in enthalpy are observed upon metal site saturation, due to more pronounced adsorbate−adsorbate interactions as the pore begins to fill with gas molecules.[50] This analysis reveals Fe_2(*m*-dobdc) to have the largest ethylene and propylene adsorption enthalpy relative to the other metal variants. At a loading of 1 mmol/g, where the differential enthalpies primarily arise from the interaction between the adsorbate and the metal site, Fe_2(*m*-dobdc) shows an ethylene adsorption of about −52 ± 0.1 kJ/mol and a propylene adsorption of −65 ± 0.5 kJ/mol.

Ethylene adsorption enthalpy magnitudes follow the trend Fe ≈ Ni ≈ 52 kJ/mol > Mn ≈ Co ≈ 47 kJ/mol. Interestingly, these are not consistent with the trend in IAST selectivity. The explanation for this discrepancy lies in the ethane adsorption enthalpies. While Ni_2(*m*-dobdc) and Fe_2(*m*-dobdc) have similar ethylene adsorption enthalpies, the ethane adsorption

DOI: 10.1021/jacs.7b06397
J. Am. Chem. Soc. 2017, 139, 15363−15370

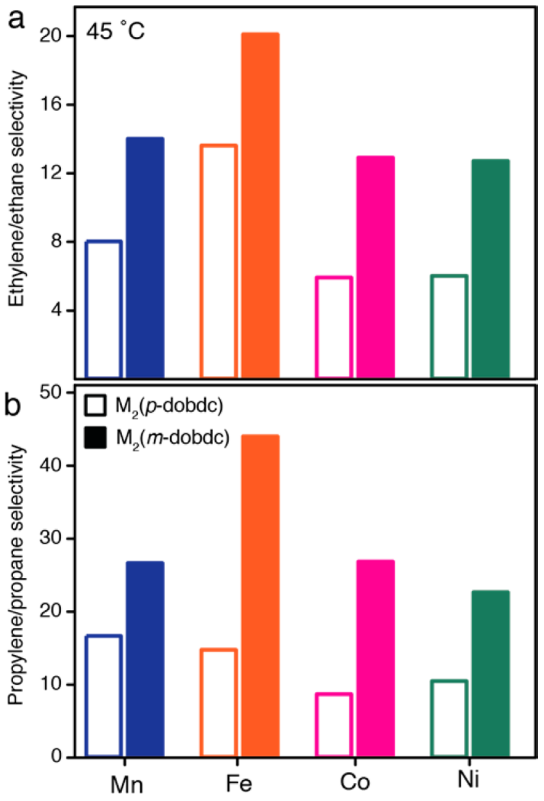

Figure 3. Comparison of the IAST selectivity under an equimolar feed at 45 °C between M_2(*p*-dobdc) and M_2(*m*-dobdc) (M = Mn, Fe, Co, Ni) for (a) ethylene/ethane and (b) propylene/propane separations.

enthalpy in Ni_2(*m*-dobdc) is ~5 kJ/mol greater than in Fe_2(*m*-dobdc). Selectivity is associated with the difference in adsorption enthalpy rather than the absolute enthalpy of the more strongly adsorbed component. This results in the Fe_2(*m*-dobdc) analog having the highest ethylene/ethane selectivity. Relatedly, Fe_2(*m*-dobdc) shows both the strongest propylene adsorption and also the highest difference in enthalpy between propylene and propane, leading to its high propylene/propane selectivity.

This metal-dependence can also be explained by a convolution of cation charge density and backbonding character. As the hard Ni^{2+} center polarizes olefins and paraffins strongly, both adsorbates show high adsorption enthalpies. Conversely, the softer Fe^{2+} cation does not polarize olefins or paraffins as strongly as Ni^{2+}, but can show enhanced backbonding interactions uniquely with olefins.

Along with olefin/paraffin selectivity, the kinetics of olefin adsorption is a crucial factor when evaluating adsorbents for industrial separations. To probe the kinetics of olefin adsorption, a transient volumetric measurement of ethylene uptake in Fe_2(*m*-dobdc) was conducted by dosing 1000 mbar of ethylene from a reservoir to the adsorbent and monitoring the pressure drop to an equilibrated pressure of 270 mbar. The resulting transient adsorption profile (Figure 5) revealed rapid

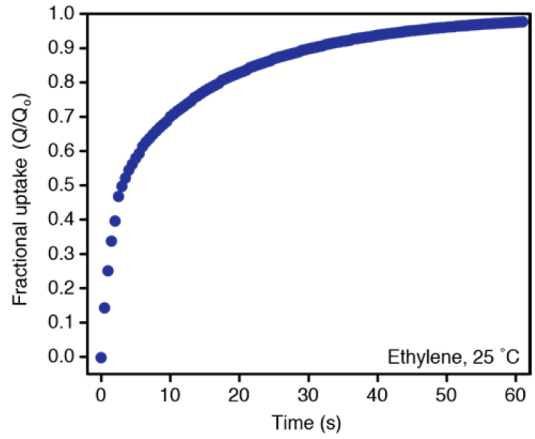

Figure 5. Transient adsorption measurement for ethylene in Fe_2(*m*-dobdc); the equilibrium pressure is ~300 mbar corresponding to an equilibrated loading (Q_0) of ~6 mmol/g.

adsorption kinetics, reaching >90% of equilibrium in less than 30 s, with complete adsorption observed in just 60 s. Thus, fast cycle times can be used in a pressure-swing adsorption process, minimizing the amount of adsorbent needed to process a given flow of gas. This fast adsorption behavior distinctly contrasts with adsorbents that rely on a size-exclusion mechanism for separating gases, in which separation occurs far from equilibrium in a real process. These findings also emphasize the advantage of adsorbents displaying fast kinetics, as pure-

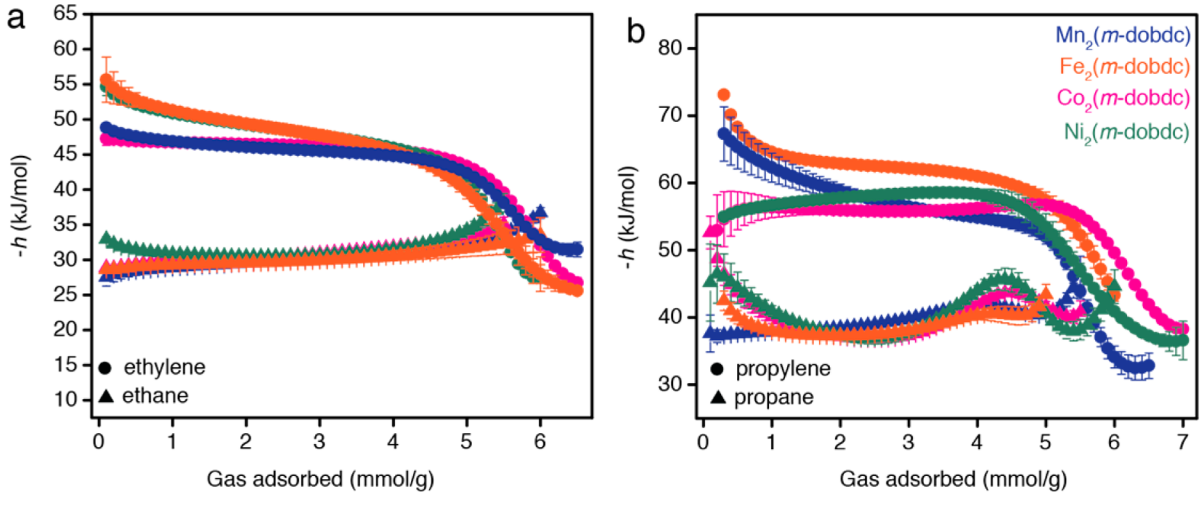

Figure 4. Differential enthalpies of adsorption for (a) ethylene and ethane and (b) propylene and propane in M_2(*m*-dobdc) (M = Mn, Fe, Co, Ni).

DOI: 10.1021/jacs.7b06397
J. Am. Chem. Soc. 2017, 139, 15363−15370

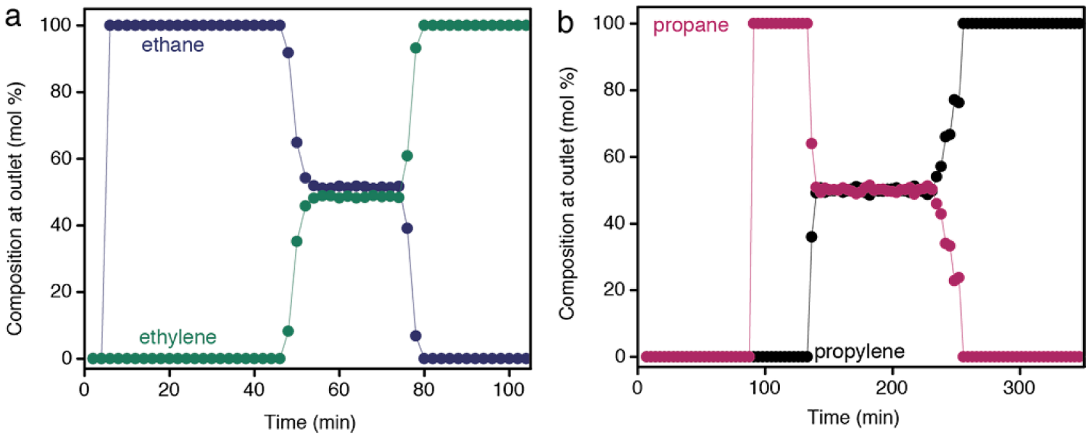

Figure 6. Transient breakthrough measurements of an equimolar mixture of (a) ethylene/ethane and (b) propylene/propane in Co_2(*m*-dobdc) at 45 °C. Breakthrough corresponds to the time when the olefin composition goes to approximately 50% of the total outflow from the packed bed. The subsequent uptick in olefin concentration corresponds to a change in the feed composition to 100% He to regenerate the bed.

component equilibrium adsorption measurements for these systems can accurately model the near-equilibrium operation of the process.

Olefin/Paraffin Breakthrough Experiments. To test the applicability of the M_2(*m*-dobdc) adsorbents under more realistic process conditions, Co_2(*m*-dobdc) was tested in a breakthrough measurement. In a typical experiment, an ethylene/ethane or propylene/propane mixture was flowed through a fixed packed bed of adsorbent with He as the carrier gas. The relative time it takes for the olefin and paraffin to break through the bed indicates the ability of the adsorbent to discriminate between the two components (Figure. 6). Longer breakthrough times for the propylene/propane mixture relative to the ethylene/ethane mixture are likely due to uncertainties in the olefin/paraffin flow rate. Using an equimolar olefin/paraffin feed, it can be seen that the paraffin breaks through the bed first, followed by the olefin. The steep breakthrough of ethane, propane, ethylene, and propylene indicates that there is a clean separation of each species. After breakthrough of both components, when the bed is saturated with an equilibrium composition, the effluent composition returns to equimolar. A subsequent purge with He at ambient conditions regenerated the bed. Notably, residual paraffin in the bed shortly after switching to desorption was not observed, indicating that the adsorbed phase is highly enriched in olefin. This implies that during olefin separation, high purity ethylene or propylene can be produced, exceeding the purity requirement of 99.9%. Additionally, the rapid desorption of the olefin by merely purging with He indicates that the olefin is labile and regeneration of the bed can be accomplished without a temperature swing. This is significant, as flowing a purge gas or using a vacuum or pressure swing are desirable over a temperature swing process, which has longer cycle times due to the time-consuming heating and cooling steps.

CONCLUSIONS

Olefin/paraffin separations account for an enormous amount of energy consumed in the industrial sector and represent a major opportunity for new adsorbents to replace cryogenic distillation. Competitive adsorbent-based technologies require materials with high selectivity and capacity, fast kinetics, labile desorption, and low production cost. We have demonstrated these key features in M_2(*m*-dobdc) (M = Mn, Fe, Co, Ni). Specifically, single-component adsorption isotherms combined with IAST reveal ethylene/ethane and propylene/propane selectivities at 25 °C in excess of 25 and 55, respectively. These selectivities arise from differences in adsorption enthalpy between olefins and paraffins, in which olefins bind more strongly at the coordinatively unsaturated metal sites present at high concentration in these materials. This separation mechanism does not rely on size exclusion and thus retains the excellent adsorption kinetics necessary for fast cycling. Notably, stronger olefin adsorption arising from increased charge density at the metal site leads to much higher selectivity in the M_2(*m*-dobdc) frameworks relative to their structural isomers, M_2(*p*-dobdc). Finally, this separation capability was demonstrated in breakthrough measurements, in which high olefin purities under mild regeneration conditions were obtained. These unique properties make the M_2(*m*-dobdc) compounds the adsorbents of choice for industrial olefin/paraffin separations and indicate a promising route to improving separation properties by tuning the electronic environment of the adsorption sites.

ASSOCIATED CONTENT

Supporting Information

The Supporting Information is available free of charge on the ACS Publications website at DOI: 10.1021/jacs.7b06397.

Additional experimental details, adsorption data and analysis, crystal structure information (PDF)

Crystallographic data for C_2H_4-dosed Co_2(*m*-dobdc) (CIF)

Crystallographic data for C_2H_4-dosed Co_2(*p*-dobdc) (CIF)

AUTHOR INFORMATION

Corresponding Author

*jrlong@berkeley.edu

ORCID

Jonathan E. Bachman: 0000-0002-3313-2355

Jeffrey R. Long: 0000-0002-5324-1321

Author Contributions

‖J.E.B. and M.T.K. contributed equally.

DOI: 10.1021/jacs.7b06397
J. Am. Chem. Soc. 2017, 139, 15363−15370

Notes

The authors declare the following competing financial interest(s): J.R.L. has a financial interest in Mosaic Materials, Inc., a start-up company working to commercialize metal-organic frameworks for gas separations. U.C. Berkeley has applied for a patent on the materials discussed herein, on which M.T.K. and J.R.L. are included as inventors.

■ ACKNOWLEDGMENTS

This research was supported through the Center for Gas Separations Relevant to Clean Energy Technologies, an Energy Frontier Research Center funded by the U.S. Department of Energy, Office of Science, Office of Basic Energy Sciences under Award DE-SC0001015. Single-crystal X-ray diffraction experiments were performed at Beamline 11.3.1 at the Advanced Light Source, a DoE Office of Science User Facility operated by Lawrence Berkeley National Laboratory under Contract No. DE-AC02-05CH11231.

■ REFERENCES

(1) Matar, S.; Hatch, L. F. *Chemistry of Petrochemical Processes*; Gulf Professional Publishing: MA, 2001.
(2) Kohl, A. L.; Nielsen, R. B. *Gas Purification*; Gulf Publishing Company: TX, 1997.
(3) U. S. Department of Energy. Materials for Separation Technology: Energy and Emission Reduction Opportunities (2005).
(4) Sholl, D. S.; Lively, R. P. *Nature* **2016**, *532*, 435−437.
(5) Eldridge, R. B. *Ind. Eng. Chem. Res.* **1993**, *32*, 2208−2212.
(6) Bai, P.; Jeon, M. Y.; Ren, L.; Knight, C.; Deem, M. W.; Tsapatsis, M.; Siepmann, J. I. *Nat. Commun.* **2015**, *6*, 5912.
(7) Rege, S. U.; Padin, J.; Yang, R. T. *AIChE J.* **1998**, *44*, 799−809.
(8) Ruthven, D. M.; Reyes, S. C. *Microporous Mesoporous Mater.* **2007**, *104*, 59−66.
(9) Yang, S.; Ramirez-Cuesta, A. J.; Newby, R.; Garcia-Sakai, V.; Manuel, P.; Callear, S. K.; Campbell, S. I.; Tang, C. C.; Schroder, M. *Nat. Chem.* **2014**, *7*, 121−129.
(10) Cadiau, A.; Adil, K.; Bhatt, P. M.; Belmabkhout, Y.; Eddaoudi, M. *Science* **2016**, *353*, 137−140.
(11) Yang, R. T.; Kikkinides, E. S. *AIChE J.* **1995**, *41*, 509−517.
(12) Li, B.; Zhang, Y.; Krishna, R.; Yao, K.; Han, Y.; Wu, Z.; Ma, D.; Shi, Z.; Pham, T.; Space, B.; Liu, J.; Thallapally, P. K.; Liu, J.; Chrzanowski, M.; Ma, S. *J. Am. Chem. Soc.* **2014**, *136*, 8654−8660.
(13) Zhang, Y.; Li, B.; Krishna, R.; Wu, Z.; Ma, D.; Shi, Z.; Pham, T.; Forrest, K.; Space, B.; Ma, S. *Chem. Commun.* **2015**, *51*, 2714−2717.
(14) Chang, G.; Huang, M.; Su, Y.; Xing, H.; Su, B.; Zhang, Z.; Yang, Q.; Yang, Y.; Ren, Q.; Bao, Z.; Chen, B. *Chem. Commun.* **2015**, *51*, 2859−2862.
(15) Blas, F. J.; Vega, L. F.; Gubbins, K. E. *Fluid Phase Equilib.* **1998**, *150-151*, 117−124.
(16) Aguado, S.; Bergeret, G.; Daniel, C.; Farrusseng, D. *J. Am. Chem. Soc.* **2012**, *134*, 14635−14637.
(17) Yu, C.; Cowan, M. G.; Noble, R. D.; Zhang, W. *Chem. Commun.* **2014**, *50*, 5745−5747.
(18) Bloch, E. D.; Queen, W. L.; Krishna, R.; Zadrozny, J. M.; Brown, C. M.; Long, J. R. *Science* **2012**, *335*, 1606−1610.
(19) Geier, S. J.; Mason, J. A.; Bloch, E. D.; Queen, W. L.; Hudson, M. R.; Brown, C. M.; Long, J. R. *Chem. Sci.* **2013**, *4*, 2054−2061.
(20) Da Silva, F. A.; Rodrigues, A. E. *AIChE J.* **2001**, *47*, 341−357.
(21) Bohme, U.; Barth, B.; Paula, C.; Kuhnt, A.; Schwieger, W.; Mundstock, A.; Caro, J.; Hartmann, M. *Langmuir* **2013**, *29*, 8592−8600.
(22) Ferreira, A. F. P.; Santos, J.; Plaza, M.; Lamia, N.; Loureiro, J. M.; Rodrigues, A. E. *Chem. Eng. J.* **2011**, *167*, 1−12.
(23) Yaghi, O. M.; Li, H.; Eddaoudi, M.; O'Keeffe, M. *Nature* **1999**, *402*, 276−279.
(24) Zhou, H.-C.; Long, J. R.; Yaghi, O. M. *Chem. Rev.* **2012**, *112*, 673.
(25) Herm, Z. R.; Bloch, E. D.; Long, J. R. *Chem. Mater.* **2014**, *26*, 323−338.
(26) Li, J.-R.; Sculley, J.; Zhou, H.-C. *Chem. Rev.* **2012**, *112*, 869−932.
(27) Yang, R. T. *Adsorbents: Fundamentals and Applications*; John Wiley & Sons, Inc.: NJ, 2003.
(28) Ben, T.; Ren, H.; Ma, S.; Cao, D.; Lan, J.; Jing, X.; Wang, X.; Xu, J.; Deng, F.; Simmons, J. M.; Qiu, S.; Zhu, G. *Angew. Chem.* **2009**, *121*, 9621−9624.
(29) McKetta, J. J. *Encyclopedia of Chemical Processing and Design*; Marcel Dekker Inc.: NY, 1984.
(30) Rosi, N. L.; Kim, J.; Eddaoudi, M.; Chen, B.; O'Keeffe, M.; Yaghi, O. M. *J. Am. Chem. Soc.* **2005**, *127*, 1504−1518.
(31) Caskey, S. R.; Wong-Foy, A. G.; Matzger, A. J. *J. Am. Chem. Soc.* **2008**, *130*, 10870−10871.
(32) Bloch, E. D.; Murray, L. J.; Queen, W. L.; Chavan, S.; Maximoff, S. N.; Bigi, J. P.; Krishna, R.; Peterson, V. K.; Grandjean, F.; Long, G. J.; Smit, B.; Bordiga, S.; Brown, C. M.; Long, J. R. *J. Am. Chem. Soc.* **2011**, *133*, 14814−14922.
(33) Bae, T.-S.; Lee, C. Y.; Kim, K. C.; Farha, O. M.; Nickias, P.; Hupp, J. T.; Nguyen, S. T.; Snurr, R. Q. *Angew. Chem., Int. Ed.* **2012**, *51*, 1857−1860.
(34) Kapelewski, M. T.; Geier, S. J.; Hudson, M. R.; Stuck, D.; Mason, J. A.; Nelson, J. N.; Xiao, D. J.; Hulvey, Z.; Gilmour, E.; FitzGerald, S. A.; Head-Gordon, M.; Brown, C. M.; Long, J. R. *J. Am. Chem. Soc.* **2014**, *136*, 12119−12129.
(35) DeSantis, D.; Mason, J. A.; James, B.; Long, J. R.; Veenstra, M. *Energy Fuels* **2017**, *31*, 2024−2032.
(36) Myers, A. L.; Prausnitz, J. M. *AIChE J.* **1965**, *11*, 121−127.
(37) LeVan, M. D.; Vermeulen, T. *J. Phys. Chem.* **1981**, *85*, 3247−3250.
(38) Richter, E.; Wilfried, S.; Myers, A. L. *Chem. Eng. Sci.* **1989**, *44*, 1609−1616.
(39) Rudzinski, W.; Everett, D. H. *Adsorption of Gases on Heterogeneous Surfaces*; Academic Press, Inc: CA, 1992.
(40) Gonzalez, M. I.; Mason, J. A.; Bloch, E. D.; Teat, S. J.; Gagnon, K. J.; Morrison, G. Y.; Queen, W. L.; Long, J. R. *Chem. Sci.* **2017**, *8*, 4387−4398.
(41) Sheldrick, G. M. *CELL NOW V2008/2*; Bruker AXS Inc.: 2008.
(42) Bruker Analytical X-ray Systems, Inc. *SAINT and APEX 2 Software for CCD Diffractometers*; Bruker Analytical X-ray Systems, Inc.: Madison, WI, USA, 2000.
(43) Sheldrick, G. M. *TWINABS, Version 2012/1*; University of Göttingen: 2012.
(44) Sheldrick, G. M. *Acta Crystallogr., Sect. A: Found. Crystallogr.* **2008**, *64* (1), 112−122.
(45) Sheldrick, G. M. *SHELXS*; University of Göttingen: Germany, 2014.
(46) Sheldrick, G. M. *Acta Crystallogr., Sect. A: Found. Adv.* **2015**, *71* (1), 3−8.
(47) Sheldrick, G. M. *SHELXL*; University of Göttingen: Germany, 2014.
(48) Dolomanov, O. V.; Bourhis, L. J.; Gildea, R. J.; Howard, J. A. K.; Puschmann, H. *J. Appl. Crystallogr.* **2009**, *42* (2), 339−341.
(49) Groom, C. R.; Bruno, I. J.; Lightfoot, M. P.; Ward, S. C. *Acta Crystallogr., Sect. B: Struct. Sci., Cryst. Eng. Mater.* **2016**, *72* (2), 171−179.
(50) Suzuki, M. *Fundamentals of Adsorption*; Kodansha, Ltd.: Tokyo, 1993.

DOI: 10.1021/jacs.7b06397
J. Am. Chem. Soc. 2017, 139, 15363−15370